ACS APPLIED MATERIALS & INTERFACES

Research Article

Cite This: ACS Appl. Mater. Interfaces 2019, 11, 9239−9250

www.acsami.org

Drastic Changes in Properties of Donor−Acceptor Polymers Induced by Asymmetric Structural Isomers for Application to Polymer Solar Cells

Sung Jae Jeon, Yong Woon Han, and Doo Kyung Moon*

Nano and Information Materials (NIMs) Laboratory, Department of Chemistry Engineering, Konkuk University, 120, Neungdong-ro, Gwangjin-gu, Seoul 05029, Republic of Korea

Supporting Information

ABSTRACT: Appropriate design of donor−acceptor (D-A) conjugated polymers is important for enhancing their physical, optical, and electrochemical properties. The rapid development of D-A conjugated polymers based on fullerene and nonfullerene derivatives in the past decade has led to an improvement in the performance of polymer solar cells (PSCs). In this study, we designed and synthesized two donor polymers based on the DTffBT acceptor unit, with matching optical absorption range and energy levels with fullerene ($PC_{71}BM$) and nonfullerene acceptors (ITIC and IDIC), by introducing asymmetric structural isomers of donor units. We demonstrated that materials design by structural modification dramatically affects the physical, optical, and electrochemical properties as well as the crystallinity and photovoltaic performance of the polymers. The results provide valuable insights into materials design for efficient PSCs.

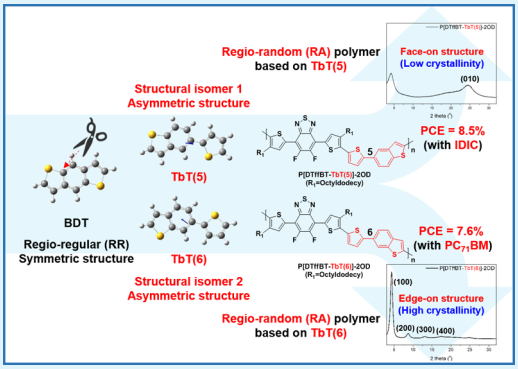

KEYWORDS: *polymer solar cells, D-A conjugated polymers, nonfullerene and fullerene, asymmetric structure*

1. INTRODUCTION

Polymer solar cells (PSCs) based on donor−acceptor (D-A) conjugated polymers are regarded as next-generation solar cells, owing to their low cost, mechanical flexibility, and suitability for use as lightweight energy sources. In addition, the ease of solution processability and abundance of raw materials make them attractive in many applications such as packaging, clothing, semitransparent windows, and portable electronics.[1−4] Single-junction PSCs have recently been reported to exhibit power conversion efficiencies (PCEs) of over 11 and 14% when fullerene and nonfullerene derivatives are used as acceptors, respectively, owing to the rapid development of D-A conjugated donor polymers.[5−10] Various molecular design strategies for D-A conjugated donor polymers have been used to tailor the molecular orbital energy levels and optical-absorption compensation ranges of specific materials to easily modulate the properties of the polymers.[11−15] In recent decades, synthetic methodologies for obtaining donor polymers, such as new building blocks,[16−18] π-conjugated spacers,[19−22] and side-chain engineering,[23−28] have been demonstrated to be very successful for optimizing the optoelectronic properties of polymers.

The development of new building blocks provides new standards and perspectives regarding the optical and electrochemical properties of donor polymers and is a noteworthy methodology. However, sometimes, an unexpected increase in the synthetic complexity of materials makes them incompatible with the PSC design requirement of low cost. It is therefore more reasonable to select donor polymers with good D-A building blocks to optimize materials using π-conjugated spacers or side-chain engineering.[6,26,29,30] However, most of these methods are ineffective because the materials are designed and synthesized from raw polymer materials by trial and error.[31,32]

Researchers are currently focusing on designing materials by considering the optical and electrochemical properties in terms of target acceptors as well as other properties such as crystallinity and miscibility.[32−36] A typical example of this type of materials design is regio-regularity control in a D-A building block.[35,37] A common regio-regular (RR) technique to obtain structurally uniform backbones in D-A conjugated polymers is to select two symmetric monomer units in the polymerization reaction. This approach can prevent structural imprecision simply by removing the possibility of regio-irregularity.[34] Hence, homogeneous donor polymers with regio-regularity have higher crystallinity and charge-carrier mobility, owing to their ordered nanostructures, and exhibit high miscibility with amorphous fullerene acceptors; this results in high-performance PSCs.[34,38]

In contrast, to realize high-performance PSCs based on nonfullerene derivatives with a coplanar and crystalline

Received: November 13, 2018
Accepted: February 14, 2019
Published: February 14, 2019

DOI: 10.1021/acsami.8b19449
ACS Appl. Mater. Interfaces 2019, 11, 9239−9250

Chart 1. DFT Calculations of BDT, TbT(5), and TbT(6) Moieties Using Gaussian 09

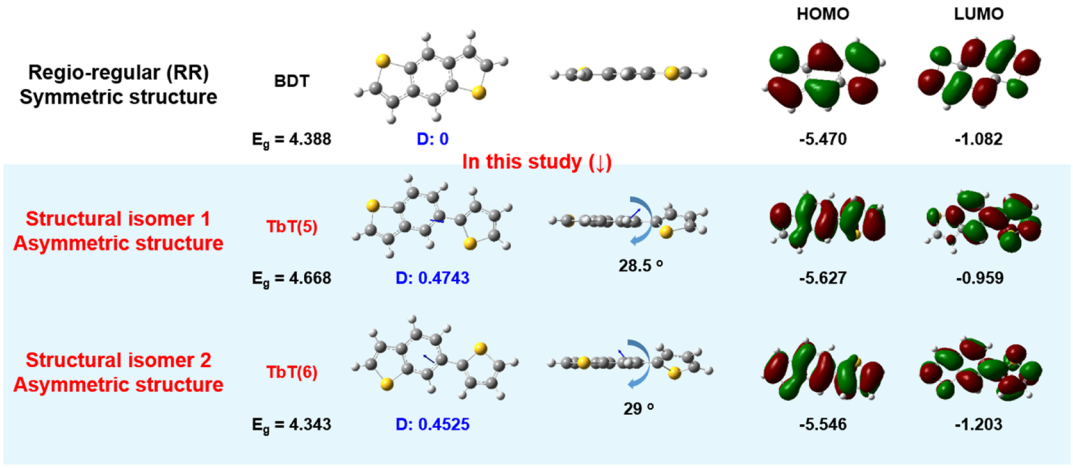

Scheme 1. Synthesis Routes of Polymers

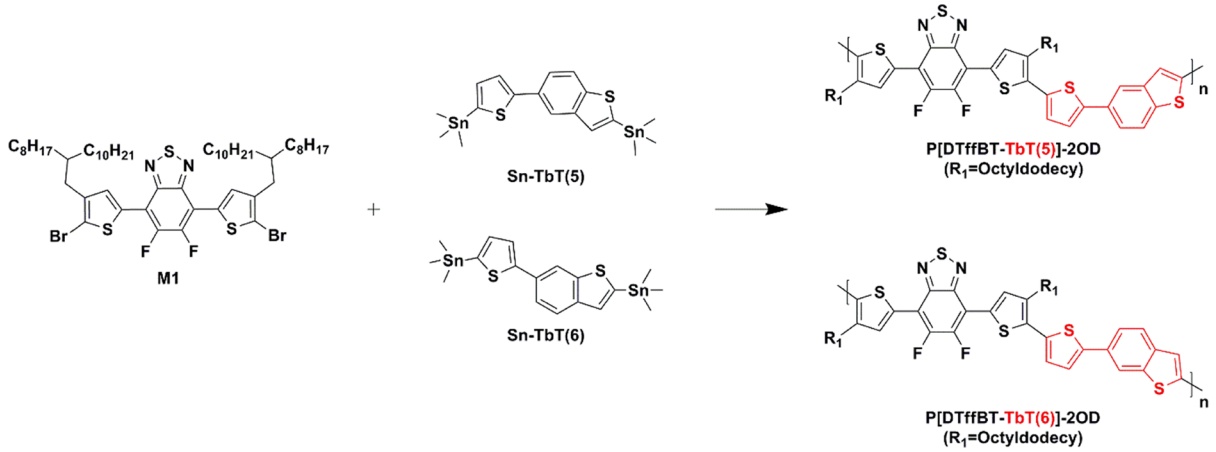

structure, a design method that can control the crystallinity of the donor polymers is needed.[33,36] Intuitively, we know that regio-random (RA) polymerization using asymmetric monomer units is effective for reducing the high crystallinity of donor polymers with an RR structure. However, this approach is not usually selected because of the preconception that efficient D-A donor polymers have RR structures and can be obtained only from donor units with symmetric structures.[32,34]

In this study, we designed and synthesized two asymmetric donor units, 5-thiophene-benzothiophene [TbT(5)] and 6-thiophene-benzothiophene [TbT(6)]. The units are structural isomers and are produced via structural modification of benzodithiophene (BDT),[14,15,17,19−21,23,26,34] an excellent RR symmetric donor unit, to effectively regulate the RA parts of the polymers. Density functional theory (DFT) calculations of BDT, TbT(5), and TbT(6) moieties were performed using Gaussian 09 before material synthesis, as summarized in Chart 1.

The dipole moment of the symmetric structure, BDT, was 0; the twisting angles in the asymmetric molecular structure were 28.5° and 29° for TbT(5) and TbT(6), respectively, and the dipole moments were calculated to be 0.4743 and 0.4525, respectively. Both moieties can be expected to have higher net dipole moments than BDT when introduced into the polymer, thus improving the short-circuit current density (J_{sc}).[32,39,40] The change in charge transport pathways due to modification of BDT to TbT(5) and TbT(6) caused extreme differences in energy levels.[34,41] Only the highest occupied molecular orbital (HOMO) level of BDT was shifted downward by 0.157 eV in TbT(5); on the other hand, in TbT(6), both HOMO and the lowest unoccupied molecular orbital (LUMO) levels were shifted downward by 0.076 and 0.121 eV, respectively. The polymer with TbT(5) can be expected to have a larger band gap, and thus a higher open-circuit voltage (V_{oc}), than the polymer with TbT(6).[34,41,42]

To study the effects of this structural modification, dithienyl difluoro-benzothiadiazole (DTffBT) substituted with an alkyl side chain, was selected as the symmetric acceptor unit in polymerization. When DTffBT is combined with various nonalkyl-substituted donor units such as thiophene and bithiophene, the polymers promote interchain interdigitation between alkyl chains.[6,30−33,36]

The RA polymers composed of DTffBT as the symmetric acceptor unit and TbT units as asymmetric donor units were structural isomers with the same conjugated D-A polymer backbone; that is, the only difference was the donor unit. However, their physical, optical, and electrochemical properties, as well as their crystallinity (orientation on the substrate), varied dramatically. The RA polymerization approach, which regulates the RA parts of the polymer backbone, makes it possible to achieve high device efficiency and high miscibility

DOI: 10.1021/acsami.8b19449
ACS Appl. Mater. Interfaces 2019, 11, 9239−9250

Table 1. Physical and Thermal Properties of Polymers

polymer	yield (%)	M_n[a] (kDa)	M_w[a] (kDa)	PDI[a]	T_d[b] (°C)	T_m[c] (°C)
P[DTffBT-TbT(5)]-2OD	65.0	25.0	35.2	1.41	400	
P[DTffBT-TbT(6)]-2OD	85.0	28.9	44.5	1.54	432	267

[a]Determined by GPC in chloroform using polystyrene standards. PDI: polydispersity index. [b]Temperature resulting in 5% weight loss based on initial weight. [c]Temperature at which polymer melts.

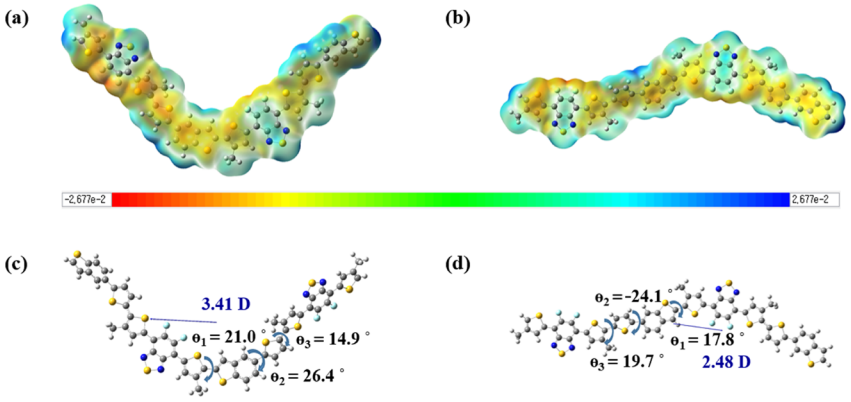

Figure 1. Calculated ESP of (a) P[DTffBT-TbT(5)]-2OD and (b) P[DTffBT-TbT(6)]-2OD at n = 2. Curvature, dipole moment, and dihedral angles of (c) P[DTffBT-TbT(5)]-2OD and (d) P[DTffBT-TbT(6)]-2OD at n = 2.

with the target acceptors by developing the asymmetric donor units TbT(5) and TbT(6).

Although the specific structure−property relationship for the development of RA D-A donor polymers has not yet been established, modification of the structural geometry of the polymer backbone can produce D-A combinations much more efficiently, along with material optimization such as the molecular weight and side-chain engineering. Thus, this study can provide insights into the use of a small number of donor units with asymmetric structures based on fullerene or nonfullerene acceptors to develop high-performance polymers.

2. EXPERIMENTAL SECTION

2.1. Polymerization. Scheme 1 outlines the synthetic routes of the polymers. Detailed synthetic procedures and characterization results for the monomers [Sn-TbT(5), Sn-TbT(6), and M1] and polymers {P[DTffBT-TbT(5)]-2OD and P[DTffBT-TbT(6)]-2OD} are presented in the Supporting Information (see Figures S1 to S12).

2.1.1. P[DTffBT-TbT(5)]-2OD. M1 (105.6 mg, 0.1 mmol), Sn-TbT(5) (0.0995 mmol), and $Pd(PPh_3)_4$ (8.0 mg) were successively added to a 0.5−2.0 mL microwave vial under air. The vial was capped and subjected to vacuum for 20 min. It was refilled with nitrogen gas, and then, anhydrous toluene (2.0 mL) was added to the mixture. The reactor was degassed and refilled with nitrogen twice. The polymerization mixture was stirred and stepwise-heated at 100 °C (10 min), 140 °C (10 min), and 160 °C (2 h) in a microwave system. The polymer was end-capped by the addition of 2-bromothiophene (0.03 g, 0.177 mmol), and the mixture was further heated at 140 °C (20 min). Then, 2-tributylstannyl thiophene (0.017 g, 0.047 mmol) was added, and the mixture was heated at 140 °C (20 min). The reaction mixture was cooled to room temperature, poured into methanol (300 mL) and 37% HCl (10 mL), and further purified by successive Soxhlet extractions using methanol, acetone, hexane, ethyl acetate, and chloroform for 24 h each. The chloroform fraction of P[DTffBT-TbT(5)]-2OD was reprecipitated in methanol, filtered, and dried under vacuum. P[DTffBT-TbT(6)]-2OD was synthesized by following the same procedure.

P[DTffBT-TbT(5)]-2OD (violet solid, yield: 65%): ^{1}H NMR (400 MHz, $CDCl_3$, δ): 7.72−7.31 (br, 6H), 7.20−6.79 (br, 2H), 2.62−2.55 (br, 4H), 1.89−1.80 (br, 2H), 1.47−0.62 (br, 76H). Anal. calcd. found (%) for $C_{66}H_{92}F_2N_2S_5$: C, 71.30; H, 8.34; F, 3.42; N, 2.52; S, 14.42; elemental analysis (EA), found (%): C, 70.65; H, 8.61; N, 2.77; S, 15.97.

P[DTffBT-TbT(6)]-2OD (dark green solid, yield: 85%): ^{1}H NMR (400 MHz, $CDCl_3$, δ): 8.10−7.31 (br, 6H), 7.20−6.95 (br, 2H), 3.64−3.53 (br, 4H), 2.04−2.00 (br, 2H), 1.47−0.70 (br, 76H). Anal. calcd. found (%) for $C_{66}H_{92}F_2N_2S_5$: C, 71.30; H, 8.34; F, 3.42; N, 2.52; S, 14.42; elemental analysis (EA), found (%): C, 70.98; H, 8.49; N, 2.59; S, 15.63.

3. RESULTS AND DISCUSSION

3.1. Materials Design and Physical Properties. The designed D-A conjugated polymers P[DTffBT-TbT(5)]-2OD and P[DTffBT-TbT(6)]-2OD were synthesized using 2-octyldodecyl-substituted DTffBT as the symmetric acceptor unit and structural isomers of TbT [TbT(5) and TbT(6)] as the asymmetric donor units. Two polymers have the same polymer backbone and differ only in the 5- or 6-position of the structural isomer TbT units. However, a close examination reveals that two polymers have distinct structural complexity in the RA polymerization behavior.[28,29,32,36,37] As shown in Figure S13, the dihedral angles between thiophene and benzothiophene in the TbT(5) and TbT(6) units were calculated; both structures showed the minimized total energy at 30° and 150°, indicating that they have two stable structures.[45] Therefore, as shown in Figures S14 and S15, the TbT units in the D-A polymer backbone are preferentially the A- or B-type. If we extend this concept to a repeating unit, where n = 4, both polymers have six model molecules, that is, six possible conformations and curvatures, excluding overlapped conformations (A/A/A/A, A/A/B/B, A/B/A/B, A/B/A/A, B/B/A/B, and B/B/B/B).[46] When TbT(6) is introduced, all of the curvatures of P[DTffBT-TbT(6)]-2OD are consistent with a linear backbone, which has low structural complexity, whereas for TbT(5), the curvatures of P[DTffBT-TbT(5)]-2OD indicate relatively high structural complexity because they have curved backbones with different forms.[34,38,47,48] Therefore, the alkyl side chains of P[DTffBT-TbT(6)]-2OD are aligned by alkyl side-chain interdigitation, and the polymer is very likely to have high crystallinity.[30,32,34] In contrast,

DOI: 10.1021/acsami.8b19449
ACS Appl. Mater. Interfaces 2019, 11, 9239−9250

P[DTffBT-TbT(5)]-2OD is likely to be amorphous or have relatively low crystallinity because the alkyl side-chain arrangements are randomly distributed.[33,34,47−49]

The molecular weights of the polymers were determined by gel permeation chromatography (GPC) using chloroform as the eluent at room temperature. The results are shown in Table 1. Both polymers have relatively high number-average molecular weights ($M_n \geq 25$ kDa).[50,51] A reasonable molecular weight can reportedly contribute to enhancement of the photovoltaic properties of polymers by altering the aggregation behavior.[52,53]

Table 1 also shows the thermal properties of these polymers, which were analyzed by thermogravimetric analysis (TGA) and differential scanning calorimetry (DSC). As shown in Figure S16, both polymers had good thermal stability over than 400 °C (5% weight-loss temperature, T_d). However, the T_d of P[DTffBT-TbT(5)]-2OD was relatively low, and its thermal stability was lower than that of P[DTffBT-TbT(6)]-2OD. The reason is that P[DTffBT-TbT(5)]-2OD is thermodynamically unstable, owing to its lower rigidity and molecular weight.[48] As shown in Figure S17, P[DTffBT-TbT(5)]-2OD showed no peak, whereas P[DTffBT-TbT(6)]-2OD showed a clear endothermic peak at 267 °C. The results indicate that P[DTffBT-TbT(5)]-2OD and P[DTffBT-TbT(6)]-2OD are amorphous and crystalline, respectively.

3.2. Computing Simulation. To investigate the π-electron systems and curvature of the polymers, computer simulation was performed using the Gaussian 09 program. To more accurately compare the conformational changes of the polymers, the curvature at $n = 2$ was calculated. In addition, the calculation time was shortened by simplifying the alkyl side chains in the polymer backbones to methyl groups. Figure 1a,b shows the calculated electrostatic surface potential (ESP) of P[DTffBT-TbT(5)]-2OD and P[DTffBT-TbT(6)]-2OD at $n = 2$; Figure 1c,d shows the curvature, dipole moments, and dihedral angles of the polymers at $n = 2$.

As shown in Figure 1a,b, both D-A polymers exhibit electron-donating behavior along the backbone, owing mainly to a positive continuous electrostatic potential of the push−pull type.[54,55] In particular, for P[DTffBT-TbT(5)]-2OD, which has a relatively curved curvature and a dense intramolecular electric field within the repeating units, a larger dipole moment can be expected compared to P[DTffBT-TbT(6)]-2OD, which has a linear curvature.[32,39,56] As shown in Figure 1c,d, the calculated dipole moment of P[DTffBT-TbT(5)]-2OD for $n = 2$ is 3.41, which is 0.93 higher than that of P[DTffBT-TbT(6)]-2OD. The calculated dihedral angles between 3-alkyl-substituted thiophene and benzothiophene (θ_1), benzothiophene and thiophene (θ_2), and thiophene and 3-alkyl-substituted thiophene (θ_3) are shown in Table 2. In particular, the curvature of the polymers is different because the direction of θ_2 differs significantly. P[DTffBT-TbT(5)]-2OD has a curved curvature because θ_1, θ_2, and θ_3 are tilted in the positive direction, whereas P[DTffBT-TbT(6)]-2OD shows a linear curvature because θ_2 is tilted in the negative direction.

Table 2. Calculated Dihedral Angles and Dipole Moments of Polymers ($n = 2$)

polymer ($n = 2$)	θ_1[a] (°)	θ_2[b] (°)	θ_3[c] (°)	dipole moment (D)
P[DTffBT-TbT(5)]-2OD	21.0	26.4	14.9	3.41
P[DTffBT-TbT(6)]-2OD	17.8	−24.1	19.7	2.48

[a]Dihedral angle between 3-alkyl-substituted-thiophene and benzothiophene. [b]Dihedral angle between benzothiophene and thiophene. [c]Dihedral angle between thiophene and 3-alkyl-substituted thiophene.

3.3. DFT Calculations. To further understand the influence of the structural difference between the polymers, optimal molecular geometries with the LUMO and HOMO levels at $n = 2$, as well as the extended conjugated curvatures of the polymers at $n = 4$, were obtained by DFT calculations using Gaussian 09. To reduce the computation time, the alkyl side chain was simplified to a methyl group. As shown in Figure 2a,b, the electron clouds of both polymers are delocalized along the entire dimer backbone, that is, in both DTffBT and TbT units, in the HOMO, whereas in the LUMO, the electron clouds of both polymers are localized in the DTffBT unit, which has relatively strong electron-withdrawing characteristics.[48,53,55] In other words, these states provide further evidence of the formation of a well-defined D-A structure and intermolecular charge transfer behavior in the polymer.[24,38,55] The calculated HOMO and LUMO energy levels and band gaps of the polymers are summarized in Table 3. The band gap of P[DTffBT-TbT(5)]-2OD is 0.122 eV larger than that of P[DTffBT-TbT(6)]-2OD. In addition, the LUMO levels of the polymers are similar, but the HOMO level of P[DTffBT-TbT(5)]-2OD (−5.008 eV) is 0.11 eV lower than that of P[DTffBT-TbT(6)]-2OD (−4.898 eV). P[DTffBT-TbT(5)]-2OD can be expected to have a higher V_{oc} than P[DTffBT-TbT(6)]-2OD when mixed with target acceptors.[41,45,46,57] As shown in Figure 2c, the curvature of the polymers at $n = 4$ is consistent with the prediction from the materials design and previous calculation data at $n = 2$. These results show that the molecular packing properties of P[DTffBT-TbT(5)]-2OD and P[DTffBT-TbT(6)]-2OD will be very different.

3.4. Optical and Electrochemical Properties. The optical properties of the polymers were investigated in both chloroform and thin films, as displayed in Figure 3. Figure 3a shows the molar absorption coefficients of the polymers measured in 10^{-5} M chloroform solutions. Figure 3b shows the UV−vis absorption spectra of the polymers in chloroform solutions and thin films, and Figure 3c shows the UV−vis absorption spectra of the polymers, ITIC, IDIC, and $PC_{71}BM$ in chloroform thin films. All the polymers exhibit two absorption bands: the first is located near 400 nm and can be assigned to intrinsic absorption of the TbT units (Figure S18) and localized $\pi-\pi^*$ transitions; the second, broader band in the long-wavelength region (beyond 500 nm) corresponds to intramolecular charge transfer (ICT) between DTffBT and TbT units.[32,45,46,58,59] However, the maximized absorption wavelength regions of the polymers were different. Specifically, P[DTffBT-TbT(5)]-2OD showed a maximized absorption wavelength in the short-wavelength range, whereas P-[DTffBT-TbT(6)]-2OD showed a maximized absorption wavelength in the long-wavelength range. This is because the two polymers, which were synthesized through structural modulation, have different curvatures, resulting in a difference in intermolecular aggregation.[20,24,25,34,38,41,47,48,60] From Figure 3a and the Beer−Lambert equation ($A = \varepsilon bc$, where A is the absorbance, ε is the molar absorption coefficient of the dye, b is the length of the light path, and c is the concentration of the dye in solution), the ε values of the polymers were calculated using the molecular weight of the repeating unit. All the molar absorption coefficients of the polymers are an average of measurements taken in four different 10^{-5} M chloroform solutions. For P[DTffBT-TbT(5)]-2OD, the ε values were

DOI: 10.1021/acsami.8b19449
ACS Appl. Mater. Interfaces 2019, 11, 9239−9250

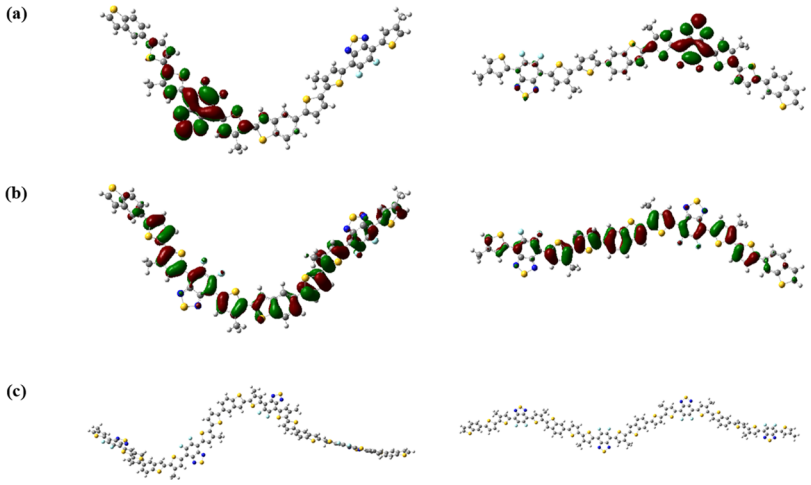

Figure 2. Optimal molecular geometries and curvature of P[DTffBT-TbT(5)]-2OD and P[DTffBT-TbT(6)] from DFT calculation: (a) LUMO and (b) HOMO at n = 2 and (c) extended conjugated curvature at n = 4.

Table 3. Results of DFT Calculation of Polymers (n = 2)

polymer (n = 2)	HOMO (eV)	LUMO (eV)	E_g (eV)
P[DTffBT-TbT(5)]-2OD	−5.008	−2.844	2.164
P[DTffBT-TbT(6)]-2OD	−4.898	−2.856	2.042

41,480 and 32,048 M^{-1} cm^{-1} at λ_{max} values of 385 and 530 nm, respectively, whereas for P[DTffBT-TbT(6)]-2OD, the ε values were 28,761, 38,331, and 36,893 M^{-1} cm^{-1} at λ_{max} values of 435, 600, and 652 nm, respectively. Both polymers had reasonable molar absorption coefficient values of approximately 30,000 M^{-1} cm^{-1} at the maximized wavelength; thus, high harvesting of photons and short-circuit current density (J_{sc}) can be expected.[34,38,45,55,59,60] As shown in Figure 3b, the main absorption peaks of the polymers showed red shift and broader absorption in the thin-film state than in the solution state. In particular, P[DTffBT-TbT(5)]-2OD was red-shifted by 40 nm more than P[DTffBT-TbT(6)]-2OD. The reason is that the intermolecular distance of P[DTffBT-TbT(5)]-2OD, which has a curved curvature, is longer than that of P[DTffBT-TbT(6)]-2OD, which has a linear curvature, in the solution state; in addition, the ICT effect is stronger, owing to high stacking and aggregation in the thin-film state.[24,25,48] Figure 3c shows the normalized UV−vis spectra of chloroform thin films of the donor polymers and acceptors used in this study. The optical band gaps of P[DTffBT-TbT(5)]-2OD, P[DTffBT-TbT(6)]-2OD, ITIC, IDIC, and $PC_{71}BM$ are 1.83, 1.72, 1.60, 1.55, and 1.90 eV, respectively, and both polymers showed a complementary optical-absorption relationship with the fullerene ($PC_{71}BM$, with broad absorption at 300 to 650 nm) and nonfullerene acceptors (ITIC and IDIC, with long-wavelength absorption at 600 to 800 nm).[43,59,61] Detailed results are given in Table 4.

To investigate the effects of electrochemical properties on the frontier energy levels of the polymers, cyclic voltammetry (CV) analysis was performed; the results are shown in Figure S19a. The HOMO and LUMO energy levels of the polymers were determined from the onset oxidation potential (E_{ox}^{onset}) and E_g − E_{HOMO} according to the electrochemical equation E_{HOMO} = −4.8 − (E_{ox}^{onset} − $E_{1/2,ferrocene}$) and are listed in Table 4. The HOMO energy level of P[DTffBT-TbT(5)]-2OD is −5.55 eV, which is 0.20 eV lower than that of P[DTffBT-TbT(6)]-2OD (−5.35 eV). The reason is that the polymer backbone incorporating the TbT(5) unit has a relatively curved structure compared to that containing the TbT(6) unit, resulting in a large tilt in the molecular structure, which affects the orbital−orbital overlap environment.[24,25,44,47,48,60] This is consistent with the results of DFT calculations. The relatively deep-lying HOMO level of P[DTffBT-TbT(5)]-2OD can contribute to the improved V_{oc} when it is mixed with target acceptors.[45,47,48] For a clear comparison, the energy level diagrams of the polymers, ITIC, IDIC, and $PC_{71}BM$ in inverted PSCs are summarized in Figure S19b.

3.5. Photovoltaic Performance. The photovoltaic performance was investigated using an inverted device config-

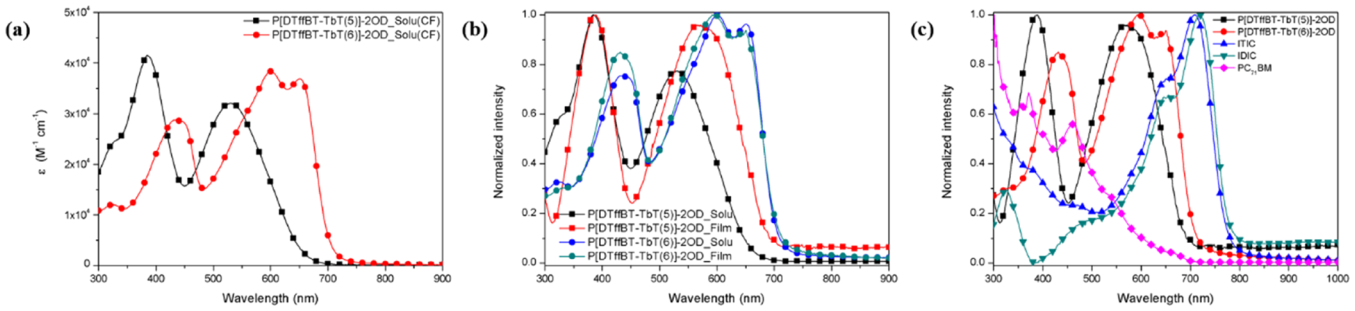

Figure 3. UV−vis absorption spectra of the polymers: (a) molar absorption coefficients in dilute chloroform solutions, (b) UV−vis absorption spectra in chloroform solutions and thin films, and (c) UV−vis absorption spectra of the polymers, ITIC, IDIC, and $PC_{71}BM$ in chloroform thin films.

DOI: 10.1021/acsami.8b19449
ACS Appl. Mater. Interfaces 2019, 11, 9239−9250

Table 4. Optical and Electrochemical Properties of Polymers

polymer	UV−visible absorption: chloroformsolution, λ_{max} (nm)	UV−visible absorption: molarabsorptioncoefficient (ε, M^{-1} cm^{-1}) at λ_{max} (nm)	UV−visible absorption: film, λ_{max} (nm)	cyclic voltammetry: E_g^{opt}[a] (eV)	cyclic voltammetry: E_{ox}^{onset} (V)	cyclic voltammetry: E_{HOMO}[b] (eV)	cyclic voltammetry: E_{LUMO}[b] (eV)
P[DTffBT-TbT(5)]-2OD	385, 530	41,480 (385), 32,048 (530)	389, 572	1.83	1.20	−5.55	−3.72
P[DTffBT-TbT(6)]-2OD	435, 600, 652	28,761 (435), 38,331 (600), 36,893 (649)	431, 592, 650	1.72	1.00	−5.35	−3.63

[a]Calculated from the intersection of the tangent on the low-energy edge of the absorption spectrum with the baseline. [b]$E_{HOMO} = -[E_{onset}$(vs Ag/AgCl) $- E_{1/2}(Fc/Fc^+$ vs Ag/AgCl)] − 4.8eV, where $E_{1/2}(Fc/Fc^+$ vs Ag/AgCl) = 0.45 eV (measured data); $E_{LUMO} = E_g - E_{HOMO}$.

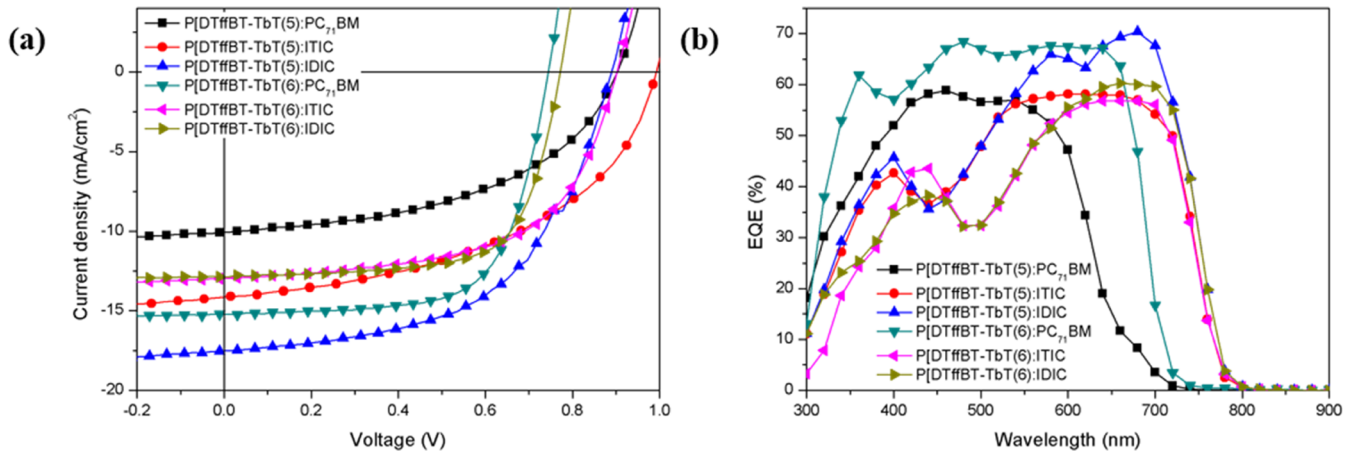

Figure 4. (a) $J-V$ and (b) EQE curves of optimized polymer blends for inverted PSCs.

Table 5. Photovoltaic Performance of Optimized Polymer Blends for Inverted PSCs

optimized conditions	V_{oc} (V)	J_{sc} (mA cm^{-2})	FF (%)	PCE_{max}/PCE_{ave}[a] (%)
P[DTffBT-TbT(5)]-2OD:$PC_{71}BM$ = 1:1.5	0.899 (0.879 ± 0.02)	10.1 (9.9 ± 0.12)	48.8 (48.3 ± 0.51)	4.4[b] (4.2 ± 0.21)
P[DTffBT-TbT(5)]-2OD:ITIC = 1:1	0.985 (0.965 ± 0.02)	14.2 (13.9 ± 0.32)	48.7 (48.5 ± 0.20)	6.8[c] (6.5 ± 0.30)
P[DTffBT-TbT(5)]-2OD:IDIC = 1:1	0.899 (0.859 ± 0.04)	17.5 (17.0 ± 0.50)	53.7 (53.3 ± 0.43)	8.5[c] (7.8 ± 0.74)
P[DTffBT-TbT(6)]-2OD:$PC_{71}BM$ = 1:1.5	0.737 (0.717 ± 0.02)	15.2 (15.1 ± 0.11)	67.7 (67.5 ± 0.24)	7.6[d] (7.4 ± 0.20)
P[DTffBT-TbT(6)]-2OD:ITIC = 1:1	0.899 (0.899)	13.0 (12.9 ± 0.13)	59.2 (58.9 ± 0.29)	6.9[e] (6.8 ± 0.11)
P[DTffBT-TbT(6)]-2OD:IDIC = 1:1	0.778 (0.757 ± 0.02)	12.9 (12.6 ± 0.32)	68.2 (67.5 ± 0.69)	6.8[e] (6.4 ± 0.42)

[a]Average PCEs are calculated from device parameters of 10 independent cells. [b]Thickness at 80 nm. [c]Thickness at 90 nm. [d]Thickness at 200 nm. [e]Thickness at 100 nm.

uration, that is, ITO/ZnO/polymer:($PC_{71}BM$, ITIC, IDIC)/MoO_3/Ag. The current density−voltage ($J-V$) and external quantum efficiency (EQE) curves of the optimized polymer blends are shown in Figure 4a,b, and the photovoltaic performance is presented in Table 5. $PC_{71}BM$, ITIC, and IDIC were used as representative electron acceptors to evaluate the photovoltaic performance of P[DTffBT-TbT(5)]-2OD and P[DTffBT-TbT(6)]-2OD in both systems.[61,62] Chlorobenzene (CB) with 1,8-diiodooctane (DIO) as an additive was chosen as the solvent for spin coating of the polymer blend films. It is well known that DIO induces proper phase separation and good mixing between polymer donors and fullerene and nonfullerene acceptors and thus improves the performance of PSCs.[58,59,61] To optimize the photovoltaic performance of the polymers with various target acceptors, the blend ratios of donors and acceptors, concentration of the active layer solutions, and DIO content were controlled. As shown in Figure 4a and Table 5, P[DTffBT-TbT(5)]-2OD and P[DTffBT-TbT(6)]-2OD showed the maximum PCE for different target acceptors and optimized conditions. Fullerene-based polymer blends of P[DTffBT-TbT(5)]-2OD achieved a PCE of 4.4% at 80 nm, with a V_{oc} of 0.899 V, J_{sc} of 10.1 mA cm^{-2}, and fill factor (FF) of 48.8%, whereas the blend of P[DTffBT-TbT(6)]-2OD had a PCE of 7.6% at 200 nm, with a V_{oc} of 0.737 V, J_{sc} of 15.2 mA cm^{-2}, and FF of 67.7%. All the active layer solutions (polymer:$PC_{71}BM$ = 1:1.5) were prepared in CB with 3.0 vol % DIO. The total concentrations were 37.5 mg mL^{-1}. All the PSC results were acquired without any post-treatment. V_{oc} was 0.16 V higher for P[DTffBT-TbT(5)]-2OD than for P-[DTffBT-TbT(6)-2OD, owing to the offset in HOMO and LUMO energy levels between the polymers and $PC_{71}BM$.[45] On the other hand, J_{sc} was more than 5.0 mA cm^{-2} higher for P[DTffBT-TbT(6)]-2OD, owing to its lower band gap, which produced an extended light-absorbing region at long wavelengths; that is, the intensity of the photo response in the EQE curves was also higher. In fact, the fullerene-based photovoltaic properties depended on the optical properties of the polymer; a photoreaction in the long wavelength range was necessary, owing to the limited absorption region of $PC_{71}BM$ (less than 600 nm).[6,14,21,24,45] The FF of P[DTffBT-TbT(6)]-2OD was also approximately 19% higher than that of P[DTffBT-TbT(5)]-2OD; the FF is closely related to the inter/intramolecular effects of the active layer.[58,60] This is discussed

DOI: 10.1021/acsami.8b19449
ACS Appl. Mater. Interfaces 2019, 11, 9239−9250

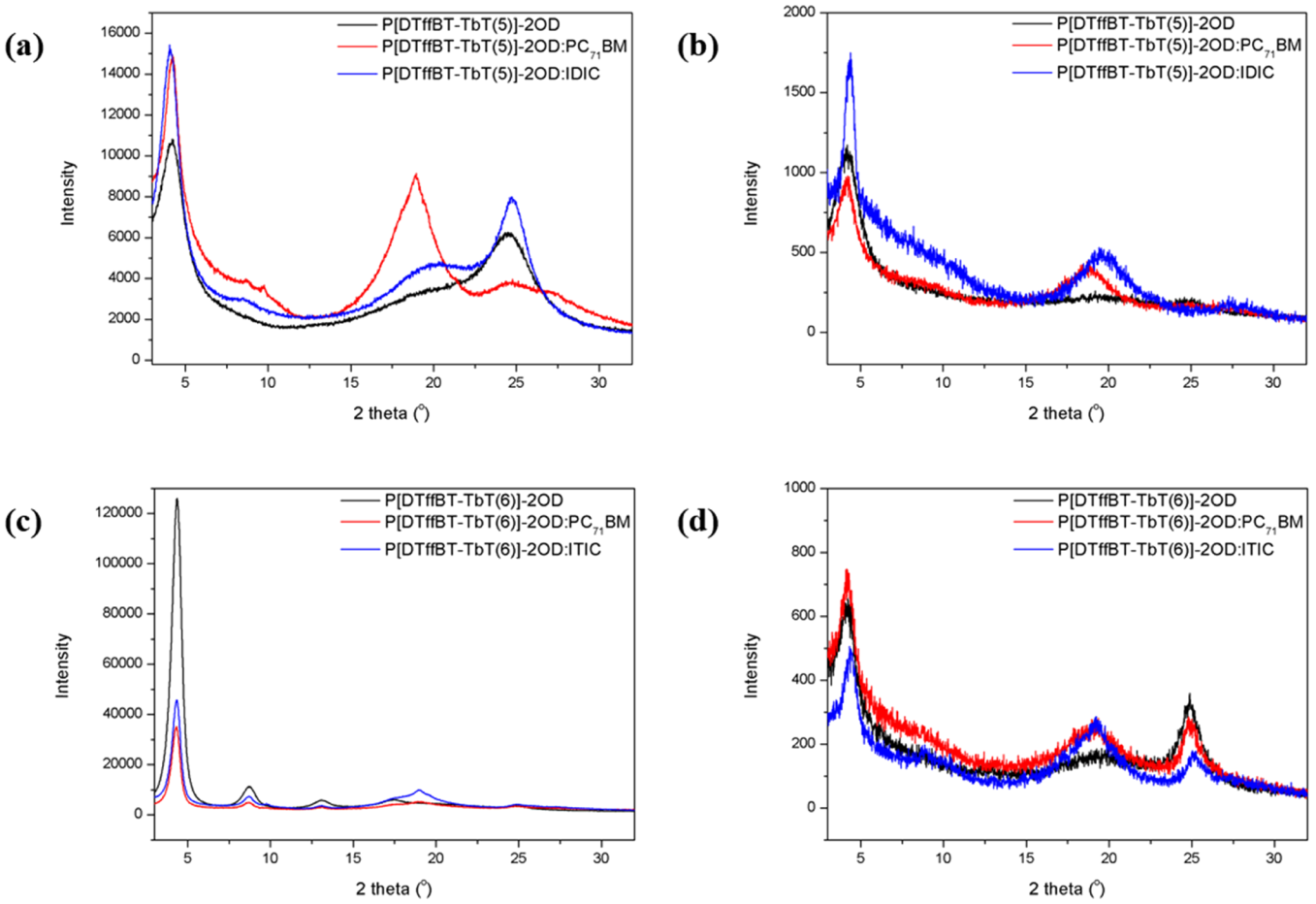

Figure 5. XRD profiles of pristine polymers and blend films: (a) out-of-plane and (b) in-plane modes for P[DTffBT-TbT(5)]-2OD; (c) out-of-plane and (d) in-plane modes for P[DTffBT-TbT(6)]-2OD.

in subsequent sections on morphology and charge-carrier transport.

In contrast, for the nonfullerene-based polymer blends, P[DTffBT-TbT(5)]-2OD exhibited better performance than P[DTffBT-TbT(6)]-2OD. Note that all the active layer solutions (polymer:ITIC or IDIC = 1:1) were prepared in CB with 0.5 vol % DIO. The active layer solutions of the polymer with IDIC blends were preheated on a hot plate at 90 °C for 30 min, owing to IDIC's low solubility in CB at room temperature. The total concentration was 20.0 mg mL^{-1}. The nonfullerene-based photoactive layers were spin-coated, followed by thermal annealing (TA) at 110 °C for 10 min. The P[DTffBT-TbT(5)]-2OD:ITIC blend had a PCE of 6.8% at 90 nm, with a V_{oc} of 0.985 V, J_{sc} of 14.2 mA cm^{-2}, and FF of 48.7%, whereas the P[DTffBT-TbT(5)]-2OD:IDIC blend had a PCE of 8.5% at 90 nm, with a V_{oc} of 0.899 V, J_{sc} of 17.5 mA cm^{-2}, and FF of 53.7%. Further, the P[DTffBT-TbT(6)]-2OD:ITIC blend had a PCE of 6.9% at 100 nm, with a V_{oc} of 0.899 V, J_{sc} of 13.0 mA cm^{-2}, and FF of 59.2%, whereas the P[DTffBT-TbT(6)]-2OD:IDIC blend had a PCE of 6.8% at 100 nm, with a V_{oc} of 0.778 V, J_{sc} of 12.9 mA cm^{-2}, and FF of 68.2%. Blends of both polymers with ITIC and IDIC were optimizable; P[DTffBT-TbT(5)]-2OD showed the best PCE in combination with IDIC, which has relatively high crystallinity, whereas P[DTffBT-TbT(6)]-2OD had the best PCE in combination with the low-crystalline ITIC.[62−65] In particular, P[DTffBT-TbT(5)]-2OD, with a deep-lying HOMO energy level, had an excellent V_{oc} of approximately 1.0 V when it was blended with ITIC. Under the optimized conditions with ITIC and IDIC, the V_{oc} values of both polymers were higher than 0.90 V, which is consistent with the difference between the HOMO energy levels of the polymers measured by CV and the LUMO energy levels of the nonfullerene acceptors.[62] J_{sc} was much higher for P[DTffBT-TbT(5)]-2OD than for P[DTffBT-TbT(6)]-2OD because P[DTffBT-TbT(5)]-2OD has a relatively larger band gap, which enhances the optical absorption compensation. The lower band gap of P[DTffBT-TbT(6)]-2OD leads to energy loss due to the overlap in the optical absorption ranges of the nonfullerene acceptors in the long-wavelength region compared to fullerene acceptors.[62,63,65] Owing to various factors such as the crystallinity, morphology, and charge-carrier transport characteristics, the FFs of the devices with both polymers were approximately 50%, which is significantly lower than the literature.[62,65] This will be explained in detail via atomic force microscopy (AFM) and space-charge-limited current (SCLC) measurement results for the fullerene-based device.

The corresponding EQE curves of the devices under optimal conditions are shown in Figure 4b. All the devices exhibited broad response ranges for the donor polymer and target acceptors. In P[DTffBT-TbT(5)]-2OD, a high J_{sc} with an EQE of more than 70% in the low-energy region (600−800 nm) contributed to the improved efficiency when the IDIC acceptor was introduced. In P[DTffBT-TbT(6)]-2OD, on the other hand, a high J_{sc} with an EQE of 65% (or higher) in all energy regions contributed to the improved efficiency when the

DOI: 10.1021/acsami.8b19449
ACS Appl. Mater. Interfaces 2019, 11, 9239−9250

Table 6. Stacking Properties for Pristine Polymers and Blend Films in Out-of-Plane Mode

film	2θ (°)/d_{100} (Å)	2θ (°)/d_{200} (Å)	2θ (°)/d_{300} (Å)	2θ (°)/d_{400} (Å)	2θ (°)/d_{010} (Å)
P[DTffBT-TbT(5)]-2OD	4.20/21.04				24.49/3.64
P[DTffBT-TbT(5)]-2OD:$PC_{71}BM$	4.22/20.94				24.54/3.63
P[DTffBT-TbT(5)]-2OD:IDIC	4.05/21.82				24.78/3.59
P[DTffBT-TbT(6)]-2OD	4.38/20.17	8.71/10.15	13.00/6.81	17.43/5.09	24.78/3.59
P[DTffBT-TbT(6)]-2OD:$PC_{71}BM$	4.33/20.41	8.74/10.10	13.10/6.76		24.81/3.59
P[DTffBT-TbT(6)]-2OD:ITIC	4.33/20.41	8.70/10.16	13.00/6.81		24.87/3.58

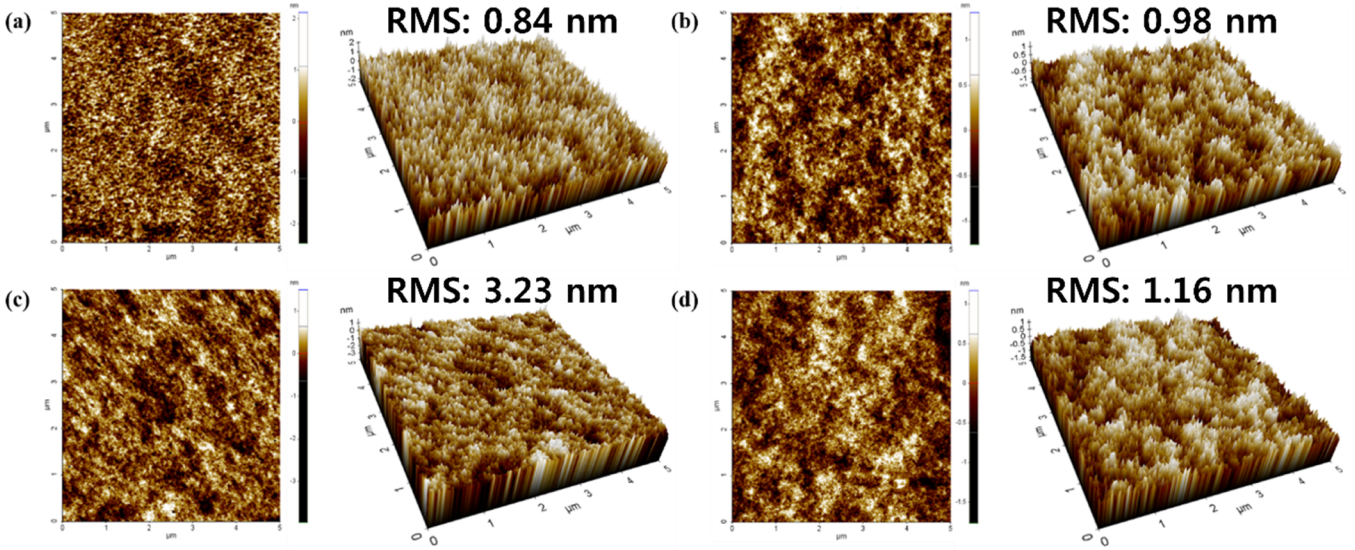

Figure 6. Images of 2D and three-dimensional (3D) topography of polymer blends: (a) P[DTffBT-TbT(5)]-2OD:$PC_{71}BM$, (b) P[DTffBT-TbT(5)]-2OD:IDIC, (c) P[DTffBT-TbT(6)]-2OD:$PC_{71}BM$, and (d) P[DTffBT-TbT(6)]-2OD:ITIC.

$PC_{71}BM$ acceptor was introduced. These results are quite consistent with the $J-V$ characteristics of the devices.

3.6. Microstructural Ordering and Morphological Characterization. The crystallinity and molecular orientations of the polymers and polymer blends with the best performance were studied by X-ray diffraction (XRD). The out-of-plane and in-plane XRD patterns of the pristine polymers and polymer blends are shown in Figure 5 and Figure S20. As shown in Figure 5a, in the out-of-plane direction, pristine P[DTffBT-TbT(5)]-2OD and the blended films show only two peaks, (100) and (010), which are related to lamellar packing and $\pi-\pi$ stacking. In the in-plane direction, the (010) peak of the pristine polymer and polymer blends disappeared, as shown in Figure 5b, indicating that the polymer has a predominantly face-on structure. The polymers retained their face-on orientation in blends with fullerene and nonfullerene acceptors.[58,61,63] In addition, the $\pi-\pi$ stacking than the blend with $PC_{71}BM$, giving the former better photovoltaic characteristics.[63] In contrast, in pristine P[DTffBT-TbT(6)]-2OD, four higher-order lamellar packing peaks were clearly detected, corresponding to the (100), (200), (300), and (400) planes, as shown in Figure 5c. In addition, as shown in Figure 5d, in the in-plane direction, the (200), (300), and (400) peaks disappear, and the (010) peak is more pronounced. Overall, this indicates that the polymer has a predominantly edge-on structure, and its relatively high crystallinity with amorphous $PC_{71}BM$ results in higher miscibility and better long-range regular packing characteristics than with ITIC.[33,65] As a result, P[DTffBT-TbT(6)]-2OD show better photovoltaic characteristics than $PC_{71}BM$.[6] Two polymers show opposite orientations on the substrate, owing to the difference in the structural isomer donor units TbT(5) and TbT(6). This is in agreement with the previously predicted change in the polymer and photovoltaic properties resulting from the curvature. The lamellar and $\pi-\pi$ stacking distances (d_{h00} and d_{010}) of the pristine polymers and polymer blends were calculated using the value of 2θ in the Bragg's law equation ($\lambda = 2d \sin\theta$; Cu, λ = 1.541871 Å; d: distance), and their values are summarized in Table 6. To examine the two-dimensional (2D) diffraction peaks of the XRD results in out-of-plane and in-plane modes, we measured the 2D grazing incidence wide-angle X-ray scattering (2D-GIWAXS) for each polymer with the best performance, as shown in Figure S21. The P[DTffBT-TbT(5)]-2OD:IDIC and P[DTffBT-TbT(6)]-2OD:$PC_{71}BM$ films showed different molecular stacking behavior and crystallization orientations. This result indicates that P[DTffBT-TbT(5)]-2OD:IDIC has a predominantly face-on structure, whereas P[DTffBT-TbT(6)]-2OD:$PC_{71}BM$ has a predominantly edge-on structure. The polymer blends exhibited high miscibility and crystallinity with each acceptor.

Tapping-mode AFM and transmission electron microscopy (TEM) were also performed to investigate the phase-separated morphologies and nanostructures of the polymer blends with fullerene and nonfullerene acceptors in the optimized PSCs. The results are shown in Figure 6 and Figure S22. The light and dark domains in the AFM and TEM images correspond to aggregation of the polymers and target acceptors, respectively.[66,67] The root-mean-square (RMS) values correlates well with observed trend in the PCEs above. The value for P[DTffBT-TbT(5)]-2OD:$PC_{71}BM$ was much lower than 1.0 nm; charge dissociation and electron movement between the polymer and $PC_{71}BM$ are inefficient, resulting in a decrease in

DOI: 10.1021/acsami.8b19449
ACS Appl. Mater. Interfaces 2019, 11, 9239−9250

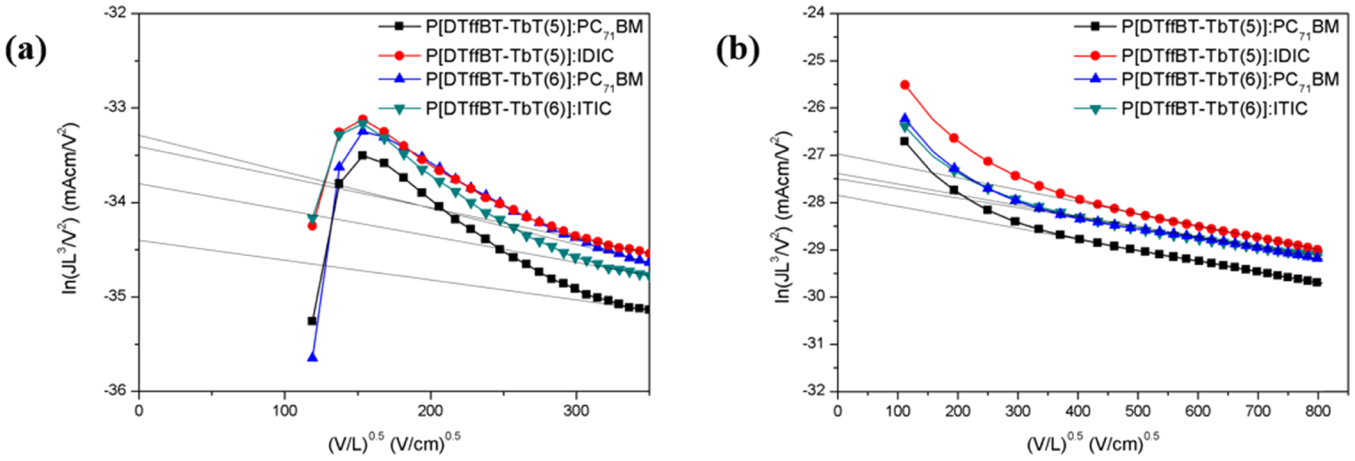

Figure 7. SCLC curves of polymer blends: (a) hole and (b) electron mobility.

Table 7. Hole and Electron Mobility of Polymer Blends

optimized conditions	μ_h ($cm^2\ V^{-1}\ s^{-1}$)	μ_e ($cm^2\ V^{-1}\ s^{-1}$)	μ_e/μ_h
P[DTffBT-TbT(5)]-2OD:$PC_{71}BM$ = 1:1.5	1.05×10^{-5}	1.07×10^{-4}	10.20
P[DTffBT-TbT(5)]-2OD:IDIC = 1:1	8.13×10^{-5}	4.34×10^{-4}	5.34
P[DTffBT-TbT(6)]-2OD:$PC_{71}BM$ = 1:1.5	8.56×10^{-5}	2.56×10^{-4}	2.99
P[DTffBT-TbT(6)]-2OD:ITIC =1:1	4.92×10^{-5}	2.53×10^{-4}	5.14

the FF.[38,58] On the other hand, P[DTffBT-TbT(6)]-2OD:$PC_{71}BM$ had efficient charge-carrier transport with an appropriate RMS value, resulting in a relatively high FF.[46,61] The difference in morphology between P[DTffBT-TbT(5)]-2OD:$PC_{71}BM$ and P[DTffBT-TbT(6)]-2OD:$PC_{71}BM$ is related mainly to the difference in their crystalline natures, induced by the incorporation of isomer TbT units, as shown in Figure 6a,c. As shown in Figure 6b,d, all the P[DTffBT-TbT(5)]-2OD:IDIC and P[DTffBT-TbT(6)]-2OD:ITIC films exhibited interpenetrating features with a bicontinuous network of donor polymers and nonfullerene acceptors. Both polymer phases had an appropriate RMS value of approximately 1.0 nm, allowing efficient charge separation between the donor and nonfullerene acceptor interfaces.[59,62] However, both film morphologies showed macrophases in which the donor polymers or nonfullerene acceptors formed large aggregates.[35] As a result, the probability of recombination after charge generation at the donor and acceptor interfaces is high.[65]

As shown in Figure S22, phase separation of the polymer blends can be clearly observed in TEM images. The four blend films exhibited different networks. First, P[DTffBT-TbT(5)]-2OD:$PC_{71}BM$ showed macrophase separation and nanostructures with poor polymer aggregation (the bright regions). Charge transfer between the donor and acceptor is difficult, so the FF and PCE are low. However, P[DTffBT-TbT(5)]-2OD:IDIC showed improved nanophase separation with a better bicontinuous interpenetrating network, which facilitates charge transfer and results in the excellent FF, J_{sc}, and PCE. In contrast, P[DTffBT-TbT(6)]-2OD:ITIC showed excessive aggregation and their domain sizes of more than 30 nm, which caused charge-carrier recombination. Finally, P[DTffBT-TbT(6)]-2OD:$PC_{71}BM$ showed nanophase separation with continuously connected nanodomain networks. Thus, it had the highest FF among the polymer blends.

3.7. Charge-Carrier Transport Properties. The charge-carrier mobility was measured to investigate balanced charge transport across the best devices using the SCLC method, as illustrated in Figure 7. The structure of electron-only devices was ITO/ZnO/polymer:($PC_{71}BM$, IDIC, ITIC)/Al, whereas that of hole-only devices was ITO/PEDOT:PSS/polymer:($PC_{71}BM$, IDIC, ITIC)/MoO_3/Ag. The Mott–Gurney space-charge limited current formula 1 was used to calculate the mobilities, with the results being shown in Table 7. Here, μ stands for the charge-carrier mobility, ε_0 and ε_r represent the dielectric constant of free space and the permittivity of the active layer, respectively, and V and L represent the applied voltage and thickness of the semiconductor layer, respectively.

$$J = (9/8)\mu\varepsilon_0\varepsilon_r(V^2/L^3) \quad (1)$$

All the polymers blended with the target acceptors showed relatively high hole and electron mobilities around an order of magnitude of 10^{-5}–10^{-4} $cm^2\ V^{-1}\ s^{-1}$. In particular, P[DTffBT-TbT(5)]-2OD:IDIC exhibited a higher charge-carrier mobilities than P[DTffBT-TbT(5)]-2OD:$PC_{71}BM$.[65] The reason is that P[DTffBT-TbT(5)]-2OD has low crystallinity and thus has high miscibility and improved π–π stacking characteristics when combined with IDIC.[62,63] In contrast, the highly crystalline P[DTffBT-TbT(6)]-2OD exhibited higher charge-carrier mobilities when blended with $PC_{71}BM$ than when blended with ITIC, owing to the higher miscibility and regular long-range packing characteristics.[65] The balance ratios of the charge-carrier mobilities for P[DTffBT-TbT(5)]-2OD:$PC_{71}BM$, P[DTffBT-TbT(5)]-2OD:IDIC, and P-[DTffBT-TbT(6)]-2OD:ITIC were 10.20, 5.34, and 5.14, respectively, which correspond to FF values of 48.8, 53.7, and 59.2%, respectively, as measured using the J–V characteristics of the PSC devices. On the other hand, P[DTffBT-TbT(6)]-2OD:$PC_{71}BM$ showed the highest balance ratio (2.99), which is closest to 1, and the highest FF (67.07%).[62,68] This trend agrees with the film morphology results discussed above.

3.8. Miscibility Analysis. To thoroughly compare the miscibilities of the donor and acceptor components, the surface tension (γ) between the polymer donor and acceptors was

DOI: 10.1021/acsami.8b19449
ACS Appl. Mater. Interfaces 2019, 11, 9239–9250

Table 8. Contact Angles of Water and Glycerol and Surface Tension for Active Layer Materials

surface	θ_{water} (°)	θ_{gly} (°)	γ (mN m^{-1})	χ
P[DTffBT-TbT(5)]-2OD	108.5	94.3	22.88	4.334[a]/1.085[b]/1.430[c]
P[DTffBT-TbT(6)]-2OD	109.4	91.8	25.09	3.445[a]/0.666[b]/0.941[c]
$PC_{71}BM$	85.4	71.3	47.13	
ITIC	94.6	83.1	33.93	
IDIC	93.1	81.4	35.75	

[a]γ_A is the surface tension of $PC_{71}BM$. [b]γ_A is the surface tension of ITIC. [c]γ_A is the surface tension of IDIC.

investigated. The γ values could be calculated according to the Wu model from the contact angles of two solvents (water and glycerol) on the neat films.[69] From the contact angle data in Figure S23 and Table 8, the water and glycerol contact angles of the polymers showed different trends. From these data and the corresponding γ values, we estimated the blend miscibility by Flory–Huggins interaction parameter (χ) based on the surface tension data using formula 2[70]

$$\chi = (\sqrt{\gamma_D} - \sqrt{\gamma_A})^2 \quad (2)$$

As a result, the calculated χ values of P[DTffBT-TbT(5)]-2OD blended with $PC_{71}BM$, ITIC, and IDIC are 4.334, 1.085, and 1.430, respectively, which implies that P[DTffBT-TbT(5)]-2OD:IDIC has relatively balanced miscibility, owing to the moderate surface tension between the donor and acceptor. In addition, IDIC showed stronger phase separation than ITIC due to harmony with miscibility and crystallinity.[71] Next, the γ values of P[DTffBT-TbT(6)]-2OD blended with $PC_{71}BM$, ITIC, and IDIC are 3.445, 0.666, and 0.941, respectively. Here, P[DTffBT-TbT(6)]-2OD:$PC_{71}BM$ has high miscibility, owing to the high crystalline nature of the polymer, which leads to high interfacial tension with amorphous acceptors.[72] Efficient PSCs were realized using P[DTffBT-TbT(5)]-2OD:IDIC and P[DTffBT-TbT(6)]-2OD:$PC_{71}BM$, which had balanced and high miscibility, respectively. The results are also consistent with the XRD, GIWAXS, AFM, and TEM results above.

4. CONCLUSIONS

In conclusion, we designed and synthesized two polymers based on the DTffBT acceptor unit by structural modification of the symmetric BDT unit in the D-A conjugated polymer backbone. The structural isomers of two polymers, P[DTffBT-TbT(5)]-2OD and P[DTffBT-TbT(6)]-2OD, were effectively regulated when two asymmetric donor units, TbT(5) and TbT(6), were introduced into their polymer backbones, resulting in RA polymerization and differences in structural complexity. Thus, two polymers, P[DTffBT-TbT(5)]-2OD and P[DTffBT-TbT(6)]-2OD, showed a curved curvature and linear curvature, respectively. We demonstrated that materials design by structural modification dramatically affects the physical, optical, and electrochemical properties, and even the crystallinity and photovoltaic performance, of the polymers. In particular, the polymers exhibited large differences in the optical band gap, HOMO energy level, and crystallinity. P[DTffBT-TbT(5)]-2OD (E_g, E_{HOMO}, orientation: 1.83 eV, −5.55 eV, face-on, respectively) had a larger band gap and a deeper-lying HOMO energy level than P[DTffBT-TbT(6)]-2OD (E_g, E_{HOMO}, orientation: 1.72 eV, −5.35 eV, edge-on, respectively) and showed a face-on structure with enhanced $\pi-\pi$ stacking as the crystallinity of the polymer decreases. Thus, efficiencies up to 8.5 and 7.6% were achieved for P[DTffBT-TbT(5)]-2OD:IDIC and P[DTffBT-TbT(6)]-2OD:$PC_{71}BM$ PSCs, respectively, owing to high miscibility and crystallinity. This work provides important scientific insights into the design of conjugated molecules for efficient organic electronics.

ASSOCIATED CONTENT

Supporting Information

The Supporting Information is available free of charge on the ACS Publications website at DOI: 10.1021/acsami.8b19449.

Experimental details (instruments, fabrication, and materials (^{1}H NMR and ^{13}C NMR)), computing simulation details, TGA, DSC, UV, CV, XRD, 2D-GIWAXS, TEM, and surface contact angle measurements (PDF)

AUTHOR INFORMATION

Corresponding Author

*E-mail: dkmoon@konkuk.ac.kr. Tel.: +82-2-450-3498. Fax: +82-2-444-0765.

ORCID

Doo Kyung Moon: 0000-0001-9482-7508

Notes

The authors declare no competing financial interest.

ACKNOWLEDGMENTS

This research was supported by the Korea Institute of Energy Technology Evaluation and Planning (KETEP) and the Ministry of Trade, Industry & Energy (MOTIE) of the Republic of Korea (nos. 20153010140030 and 2018201010636A).

REFERENCES

(1) Shrotriya, V. Polymer Power. *Nat. Photonics* **2009**, *3*, 447–449.

(2) Polman, A.; Knight, M.; Garnett, E. C.; Ehrler, B.; Sinke, W. C. Photovoltaic Materials: Present Efficiencies and Future Challenges. *Science* **2016**, *352*, aad4424.

(3) Lu, L.; Zheng, T.; Wu, Q.; Schneider, A. M.; Zhao, D.; Yu, L. Recent Advances in Bulk Heterojunction Polymer Solar Cells. *Chem. Rev.* **2015**, *115*, 12666–12731.

(4) Cheng, P.; Zhan, X. Stability of Organic Solar Cells: Challenges and Strategies. *Chem. Soc. Rev.* **2016**, *45*, 2544–2582.

(5) Zhao, J.; Li, Y.; Yang, G.; Jiang, K.; Lin, H.; Ade, H.; Ma, W.; Yan, H. Efficient Organic Solar Cells Processed from Hydrocarbon Solvents. *Nat. Energy* **2016**, *1*, 15027.

(6) Zhang, S.; Qin, Y.; Zhu, J.; Hou, J. Over 14% Efficiency in Polymer Solar Cells Enabled by a Chlorinated Polymer Donor. *Adv. Mater.* **2018**, *30*, 1800868.

(7) Li, H.; Xiao, Z.; Ding, L.; Wang, J. Thermostable Single-Junction Organic Solar Cells with a Power Conversion Efficiency of 14.62%. *Sci. Bull.* **2018**, *63*, 340–342.

(8) Zhang, H.; Yao, H.; Hou, J.; Zhu, J.; Zhang, J.; Li, W.; Yu, R.; Gao, B.; Zhang, S.; Hou, J. Over 14% Efficiency in Organic Solar Cells

DOI: 10.1021/acsami.8b19449
ACS Appl. Mater. Interfaces 2019, 11, 9239–9250

Enabled by Chlorinated Nonfullerene Small-Molecule Acceptors. *Adv. Mater.* **2018**, *30*, 1800613.
(9) Xiao, Z.; Jia, X.; Ding, L. Ternary Organic Solar Cells Offer 14% Power Conversion Efficiency. *Sci. Bull.* **2017**, *62*, 1562−1564.
(10) Liu, Z.; Zeng, D.; Gao, X.; Li, P.; Zhang, Q.; Peng, X. Non-Fullerene Polymer Acceptors Based on Perylene Diimides in All-Polymer Solar Cells. *Sol Energy Mater. Sol Cells.* **2019**, *189*, 103−117.
(11) Liu, Z.; Zhang, X.; Li, P.; Gao, X. Recent Development of Efficient A-D-A type Fused-Ring Electron Acceptors for Organic Solar. *Sol. Energy.* **2018**, *174*, 171−188.
(12) Liu, Z.; Zhang, L.; Shao, M.; Wu, Y.; Zeng, D.; Cai, X.; Duan, J.; Zhang, X.; Gao, X. Fine-Tuning the Quasi-3D Geometry: Enabling Efficient Nonfullerene Organic Solar Cells Based on Perylene Diimides. *ACS Appl. Mater. Interfaces* **2018**, *10*, 762−768.
(13) Yao, H.; Ye, L.; Zhang, H.; Li, S.; Zhang, S.; Hou, J. Molecular Design of Benzodithiophene-Based Organic Photovoltaic Materials. *Chem. Rev.* **2016**, *116*, 7397−7457.
(14) Cai, Y.; Huo, L.; Sun, Y. Recent Advances in Wide-Bandgap Photovoltaic Polymers. *Adv. Mater.* **2017**, *29*, 1605437.
(15) Guo, X.; Quinn, J.; Chen, Z.; Usta, H.; Zheng, Y.; Xia, Y.; Hennek, J. W.; Ortiz, R. P.; Marks, T. J.; Facchetti, A. Dialkoxybithiazole: A New Building Block for Head-to-Head Polymer Semiconductors. *J. Am. Chem. Soc.* **2013**, *135*, 1986−1996.
(16) Wang, H.; Shi, Q.; Lin, Y.; Fan, H.; Cheng, P.; Zhan, X.; Li, Y.; Zhu, D. Conjugated Polymers Based on a New Building Block: Dithienophthalimide. *Macromolecules* **2011**, *44*, 4213−4221.
(17) Guo, X.; Liao, Q.; Manley, E. F.; Wu, Z.; Wang, Y.; Wang, W.; Yang, T.; Shin, Y.-E.; Cheng, X.; Liang, Y.; Chen, L. X.; Baeg, K.-J.; Marks, T. J.; Guo, X. Materials Design via Optimized Intramolecular Noncovalent Interactions for High-Performance Organic Semiconductors. *Chem. Mater.* **2016**, *28*, 2449−2460.
(18) Dang, D.; Xiao, M.; Zhou, P.; Shi, J.; Tao, Q.; Tan, H.; Wang, Y.; Bao, X.; Liu, Y.; Wang, E.; Yang, R.; Zhu, W. Manipulating Backbone Structure with Various Conjugated Spacers to Enhance Photovoltaic Performance of D-A-Type Two-Dimensional Copolymers. *Org. Electron.* **2014**, *15*, 2876−2884.
(19) Lee, T. H.; Choi, M. H.; Jeon, S. J.; Moon, D. K. Correlation of Intermolecular Packing Distance and Crystallinity of D-A Polymers According to π-Spacer for Polymer Solar Cells. *Polymer* **2016**, *99*, 756−766.
(20) Xu, Z.; Fan, Q.; Meng, X.; Guo, X.; Su, W.; Ma, W.; Zhang, M.; Li, Y. Selenium-Containing Medium Bandgap Copolymer for Bulk Heterojunction Polymer Solar Cells with High Efficiency of 9.8%. *Chem. Mater.* **2017**, *29*, 4811−4818.
(21) Dang, D.; Zhou, P.; Duan, L.; Bao, X.; Yang, R.; Zhu, W. An Efficient Method to Achieve a Balanced Open Circuit Voltage and Short Circuit Current Density in Polymer Solar Cells. *J. Mater. Chem. A* **2016**, *4*, 8291−8297.
(22) Min, J.; Cui, C.; Heumueller, T.; Fladischer, S.; Cheng, X.; Spiecker, E.; Li, Y.; Brabec, C. J. Side-Chain Engineering for Enhancing the Properties of Small Molecule Solar Cells: A Trade-off Beyond Efficiency. *Adv. Energy Mater.* **2016**, *6*, 1600515.
(23) Huang, L.; Zhang, G.; Zhang, K.; Peng, Q.; Wong, M. S. Benzodithiophene−Dithienylbenzothiadiazole Copolymers for Efficient Polymer Solar Cells: Side-Chain Effect on Photovoltaic Performance. *ACS Appl. Mater. Interfaces* **2018**, *10*, 34355−34362.
(24) Wang, B.; Zhang, J.; Tam, H. L.; Wu, B.; Zhang, W.; Chan, M. S.; Pan, F.; Yu, G.; Zhu, F.; Wong, M. S. Impact of Alkyl Side Chains on the Photovoltaic and Charge Mobility Properties of Naphthodithiophene-Benzothiadiazole Copolymers. *Polym. Chem.* **2014**, *5*, 836−843.
(25) Yuan, J.; Qiu, L.; Zhang, Z.; Li, Y.; He, Y.; Jiang, L.; Zou, Y. A Simple Strategy to the Side Chain Functionalization on the Quinoxaline Unit for Efficient Polymer Solar Cells. *Chem. Commun.* **2016**, *52*, 6881−6884.
(26) Gao, Y.; Wang, Z.; Zhang, J.; Zhang, H.; Lu, K.; Guo, F.; Wei, Z.; Yang, Y.; Zhao, L.; Zhang, Y. Wide-Bandgap Conjugated Polymers Based on Alkylthiofuran-Substituted Benzo[1,2-b:4,5- b′]difuran for Efficient Fullerene-Free Polymer Solar Cells. *Macromolecules* **2018**, *51*, 2498−2505.
(27) Gao, Y.; Wang, Z.; Zhang, J.; Zhang, H.; Lu, K.; Guo, F.; Yang, Y.; Zhao, L.; Wei, Z.; Zhang, Y. Two-Dimensional Benzo[1,2-:b:4,5-b′]difuran-Based Wide Bandgap Conjugated Polymers for Efficient Fullerene-Free Polymer Solar Cells. *J. Mater. Chem. A* **2018**, *6*, 4023−4031.
(28) Mei, C.-Y.; Liang, L.; Zhao, F.-G.; Wang, J.-T.; Yu, L.-F.; Li, Y.-X.; Li, W.-S. A Family of Donor-Acceptor Photovoltaic Polymers with Fused 4,7-Dithienyl-2,1,3-Benzothiadiazole Units: Effect of Structural Fusion and Side Chains. *Macromolecules* **2013**, *46*, 7920−7931.
(29) Po, R.; Bianchi, G.; Carbonera, C.; Pellegrino, A. "all That Glisters Is Not Gold": An Analysis of the Synthetic Complexity of Efficient Polymer Donors for Polymer Solar Cells. *Macromolecules* **2015**, *48*, 453−461.
(30) Carlé, J. E.; Helgesen, M.; Hagemann, O.; Hösel, M.; Heckler, I. M.; Bundgaard, E.; Gevorgyan, S. A.; Søndergaard, R. R.; Jørgensen, M.; García-Valverde, R.; Chaouki-Almagro, S.; Villarejo, J. A.; Krebs, F. C. Overcoming the Scaling Lag for Polymer Solar Cells. *Joule* **2017**, *1*, 274−289.
(31) Zhang, Z.; Feng, L.; Xu, S.; Liu, Y.; Peng, H.; Zhang, Z.-G.; Li, Y.; Zou, Y. A New Electron Acceptor with Meta-Alkoxyphenyl Side Chain for Fullerene-Free Polymer Solar Cells with 9.3% Efficiency. *Adv. Sci.* **2017**, *4*, 1700152.
(32) Hu, H.; Jiang, K.; Yang, G.; Liu, J.; Li, Z.; Lin, H.; Liu, Y.; Zhao, J.; Zhang, J.; Huang, F.; Qu, Y.; Ma, W.; Yan, H. Terthiophene-Based D-A Polymer with an Asymmetric Arrangement of Alkyl Chains That Enables Efficient Polymer Solar Cells. *J. Am. Chem. Soc.* **2015**, *137*, 14149−14157.
(33) Zhang, Z.; Lu, Z.; Zhang, J.; Liu, Y.; Feng, S.; Wu, L.; Hou, R.; Xu, X.; Bo, Z. High Efficiency Polymer Solar Cells Based on Alkylthio Substituted Benzothiadiazole-Quaterthiophene Alternating Conjugated Polymers. *Org. Electron.* **2017**, *40*, 36−41.
(34) Zhou, C.; Zhang, G.; Zhong, C.; Jia, X.; Luo, P.; Xu, R.; Gao, K.; Jiang, X.; Liu, F.; Russell, T. P.; Huang, F.; Cao, Y. Toward High Efficiency Polymer Solar Cells: Influence of Local Chemical Environment and Morphology. *Adv. Energy Mater.* **2017**, *7*, 1601081.
(35) Chen, S.; Yao, H.; Li, Z.; Awartani, O. M.; Liu, Y.; Wang, Z.; Yang, G.; Zhang, J.; Ade, H.; Yan, H. Surprising Effects upon Inserting Benzene Units into a Quaterthiophene-Based D-A Polymer−Improving Non-Fullerene Organic Solar Cells via Donor Polymer Design. *Adv. Energy Mater.* **2017**, *7*, 1602304.
(36) Ying, L.; Huang, F.; Bazan, G. C. Regioregular Narrow-Bandgap-Conjugated Polymers for Plastic Electronics. *Nat. Commun.* **2017**, *8*, 14047.
(37) Wang, X.; Deng, W.; Chen, Y.; Wang, X.; Ye, P.; Wu, X.; Yan, C.; Zhan, X.; Liu, F.; Huang, H. Fine-Tuning Solid State Packing and Significantly Improving Photovoltaic Performance of Conjugated Polymers through Side Chain Engineering via Random Polymerization. *J. Mater. Chem. A* **2017**, *5*, 5585−5593.
(38) Li, Z.; Jiang, K.; Yang, G.; Lai, J. Y. L.; Ma, T.; Zhao, J.; Ma, W.; Yan, H. Donor Polymer Design Enables Efficient Non-Fullerene Organic Solar Cells. *Nat. Commun.* **2016**, *7*, 13094.
(39) Wang, M.; Cai, D.; Yin, Z.; Chen, S.-C.; Du, C.-F.; Zheng, Q. Asymmetric-Indenothiophene-Based Copolymers for Bulk Heterojunction Solar Cells with 9.14% Efficiency. *Adv. Mater.* **2016**, *28*, 3359−3365.
(40) Yuan, J.; Ford, M. J.; Zhang, Y.; Dong, H.; Li, Z.; Li, Y.; Nguyen, T.-Q.; Bazan, G. C.; Ma, W. Toward Thermal Stable and High Photovoltaic Efficiency Ternary Conjugated Copolymers: Influence of Backbone Fluorination and Regioselectivity. *Chem. Mater.* **2017**, *29*, 1758−1768.
(41) Collado-Fregoso, E.; Boufflet, P.; Fei, Z.; Gann, E.; Ashraf, S.; Li, Z.; McNeill, C. R.; Durrant, J. R.; Heeney, M. Increased Exciton Dipole Moment Translates into Charge-Transfer Excitons in Thiophene-Fluorinated Low-Bandgap Polymers for Organic Photovoltaic Applications. *Chem. Mater.* **2015**, *27*, 7934−7944.
(42) Gao, W.; Liu, T.; Zhong, C.; Zhang, G.; Zhang, Y.; Ming, R.; Zhang, L.; Xin, J.; Wu, K.; Guo, Y.; Ma, W.; Yan, H.; Liu, Y.; Yang, C.

DOI: 10.1021/acsami.8b19449
ACS Appl. Mater. Interfaces 2019, 11, 9239−9250

Asymmetrical Small Molecule Acceptor Enabling Nonfullerene Polymer Solar Cell with Fill Factor Approaching 79%. *ACS Energy Lett.* **2018**, *3*, 1760−1768.
(43) Coughlin, J. E.; Zhugayevych, A.; Wang, M.; Bazan, G. C.; Tretiak, S. Charge Delocalization Characteristics of Regioregular High Mobility Polymers. *Chem. Sci.* **2017**, *8*, 1146−1151.
(44) Xin, Y.; Zeng, G.; Zhang, J.; Zhao, X.; Yang, X. A New Copolymer Based on a D-π-A or D-A-π Repeat Unit for Polymer Solar Cells Employing Non-Halogenated Solvents. *J. Mater. Chem. A* **2018**, *6*, 9561−9568.
(45) Wan, Z.; Yang, J.; Liu, Y.; Wang, S.; Zhong, Y.; Li, C.; Zhang, Z.; Xing, G.; Huettner, S.; Tao, Y.; Li, Y.; Huang, W. Cyclometalated Pt Complex-Based Random Terpolymers for Efficient Polymer Solar Cells. *Polym. Chem.* **2017**, *8*, 4729−4737.
(46) Jeon, S. J.; Nam, S. J.; Han, Y. W.; Lee, T. H.; Moon, D. K. Molecular Design through Computational Simulation on the Benzo-[2,1- b;3,4- b ′]Dithiophene-Based Highly Ordered Donor Material for Efficient Polymer Solar Cells. *Polym. Chem.* **2017**, *8*, 2979−2989.
(47) Lee, J.; Sin, D. H.; Moon, B.; Shin, J.; Kim, H. G.; Kim, M.; Cho, K. Highly Crystalline Low-Bandgap Polymer Nanowires towards High-Performance Thick-Film Organic Solar Cells Exceeding 10% Power Conversion Efficiency. *Energy Environ. Sci.* **2017**, *10*, 247−257.
(48) Yang, J.; Chen, F.; Xiao, B.; Sun, S.; Sun, X.; Tajima, K.; Tang, A.; Zhou, E. Modulating the Symmetry of Benzodithiophene by Molecular Tailoring for the Application in Naphthalene Diimide-Based N-Type Photovoltaic Polymers. *Solar RRL* **2018**, *2*, 1700230.
(49) Cheng, S.-W.; Chiou, D.-Y.; Tsai, C.-E.; Liang, W.-W.; Lai, Y.-Y.; Hsu, J.-Y.; Hsu, C.-S.; Osaka, I.; Takimiya, K.; Cheng, Y.-J. Angular-Shaped 4,9-Dialkyl α- And β-Naphthodithiophene-Based Donor-Acceptor Copolymers: Investigation of Isomeric Structural Effects on Molecular Properties and Performance of Field-Effect Transistors and Photovoltaics. *Adv. Funct. Mater.* **2015**, *25*, 6131−6143.
(50) Yao, H.; Li, Y.; Hu, H.; Chow, P. C. Y.; Chen, S.; Zhao, J.; Li, Z.; Carpenter, J. H.; Lai, J. Y. L.; Yang, G.; Liu, Y.; Lin, H.; Ade, H.; Yan, H. A Facile Method to Fine-Tune Polymer Aggregation Properties and Blend Morphology of Polymer Solar Cells Using Donor Polymers with Randomly Distributed Alkyl Chains. *Adv. Energy Mater.* **2018**, *8*, 1701895.
(51) Yang, Y.; Mielczarek, K.; Zakhidov, A.; Hu, W. Large Molecular Weight Polymer Solar Cells with Strong Chain Alignment Created by Nanoimprint Lithography. *ACS Appl. Mater. Interfaces* **2016**, *8*, 7300−7307.
(52) Marszalek, T.; Li, M.; Pisula, W. Design Directed Self-Assembly of Donor−acceptor Polymers. *Chem. Commun.* **2016**, *52*, 10938−10947.
(53) Vangerven, T.; Verstappen, P.; Drijkoningen, J.; Dierckx, W.; Himmelberger, S.; Salleo, A.; Vanderzande, D.; Maes, W.; Manca, J. V. Molar Mass versus Polymer Solar Cell Performance: Highlighting the Role of Homocouplings. *Chem. Mater.* **2015**, *27*, 3726−3732.
(54) Lee, J.; Kim, M.; Kang, B.; Jo, S. B.; Kim, H. G.; Shin, J.; Cho, K. Side-Chain Engineering for Fine-Tuning of Energy Levels and Nanoscale Morphology in Polymer Solar Cells. *Adv. Energy Mater.* **2014**, *4*, 1400087.
(55) Luo, H.; Yu, C.; Liu, Z.; Zhang, G.; Geng, H.; Yi, Y.; Broch, K.; Hu, Y.; Sadhanala, A.; Jiang, L.; Qi, P.; Cai, Z.; Sirringhaus, H.; Zhang, D. Remarkable Enhancement of Charge Carrier Mobility of Conjugated Polymer Field-Effect Transistors upon Incorporating an Ionic Additive. *Sci. Adv.* **2016**, *2*, No. e1600076.
(56) Jin, Y.; Chen, Z.; Dong, S.; Zheng, N.; Ying, L.; Jiang, X.-F.; Liu, F.; Huang, F.; Cao, Y. A Novel Naphtho[1,2-c:5,6-C′]Bis([1,2,5]-Thiadiazole)-Based Narrow-Bandgap π-Conjugated Polymer with Power Conversion Efficiency Over 10%. *Adv. Mater.* **2016**, *28*, 9811−9818.
(57) Yao, H.; Qian, D.; Zhang, H.; Qin, Y.; Xu, B.; Cui, Y.; Yu, R.; Gao, F.; Hou, J. Critical Role of Molecular Electrostatic Potential on Charge Generation in Organic Solar Cells. *Chin. J. Chem.* **2018**, *36*, 491−494.
(58) Yuan, J.; Zou, Y.; Cui, R.; Chao, Y.-H.; Wang, Z.; Ma, M.; He, Y.; Li, Y.; Rindgen, A.; Ma, W.; Xiao, D.; Bo, Z.; Xu, X.; Li, L.; Hsu, C.-S. Incorporation of Fluorine onto Different Positions of Phenyl Substituted Benzo[1,2-b:4,5-B′]Dithiophene Unit: Influence on Photovoltaic Properties. *Macromolecules* **2015**, *48*, 4347−4356.
(59) Li, Z.; Xu, X.; Zhang, G.; Yu, T.; Li, Y.; Peng, Q. Highly Efficient Non-Fullerene Polymer Solar Cells Enabled by Wide Bandgap Copolymers With Conjugated Selenyl Side Chains. *Solar RRL* **2018**, *2*, 1800186.
(60) Chiou, D.-Y.; Cao, F.-Y.; Hsu, J.-Y.; Tsai, C.-E.; Lai, Y.-Y.; Jeng, U.-S.; Zhang, J.; Yan, H.; Su, C.-J.; Cheng, Y.-J. Synthesis and Side-Chain Isomeric Effect of 4,9-/5,10-Dialkylated-β-Angular-Shaped Naphthodithiophenes-Based Donor-Acceptor Copolymers for Polymer Solar Cells and Field-Effect Transistors. *Polym. Chem.* **2017**, *8*, 2334−2345.
(61) Guo, B.; Li, W.; Guo, X.; Meng, X.; Ma, W.; Zhang, M.; Li, Y. A Novel Wide Bandgap Conjugated Polymer (2.0 EV) Based on Bithiazole for High Efficiency Polymer Solar Cells. *Nano Energy* **2017**, *34*, 556−561.
(62) Su, W.; Fan, Q.; Guo, X.; Meng, X.; Bi, Z.; Ma, W.; Zhang, M.; Li, Y. Two Compatible Nonfullerene Acceptors with Similar Structures as Alloy for Efficient Ternary Polymer Solar Cells. *Nano Energy* **2017**, *38*, 510−517.
(63) Lin, F.; Huang, W.; Sun, H.; Xin, J.; Zeng, H.; Yang, T.; Li, M.; Zhang, X.; Ma, W.; Liang, Y. Thieno[3,4-c]Pyrrole-4,6(5H)-Dione Polymers with Optimized Energy Level Alignments for Fused-Ring Electron Acceptor Based Polymer Solar Cells. *Chem. Mater.* **2017**, *29*, 5636−5645.
(64) Jiang, H.; Wang, Z.; Zhang, L.; Zhong, A.; Liu, X.; Pan, F.; Cai, W.; Inganäs, O.; Liu, Y.; Chen, J.; Cao, Y. A Highly Crystalline Wide-Band-Gap Conjugated Polymer toward High-Performance As-Cast Nonfullerene Polymer Solar Cells. *ACS Appl. Mater. Interfaces* **2017**, *9*, 36061−36069.
(65) Li, H.; Zhao, Y.; Fang, J.; Zhu, X.; Xia, B.; Lu, K.; Wang, Z.; Zhang, J.; Guo, X.; Wei, Z. Improve the Performance of the All-Small-Molecule Nonfullerene Organic Solar Cells through Enhancing the Crystallinity of Acceptors. *Adv. Energy Mater.* **2018**, *8*, 1702377.
(66) de Zerio, A. D.; Müller, C. Glass Forming Acceptor Alloys for Highly Efficient and Thermally Stable Ternary Organic Solar Cells. *Adv. Energy Mater.* **2018**, *8*, 1702741.
(67) Li, W.; Cai, J.; Cai, F.; Yan, Y.; Yi, H.; Gurney, R. S.; Liu, D.; Iraqi, A.; Wang, T. Achieving Over 11% Power Conversion Efficiency in PffBT4T-2OD-Based Ternary Polymer Solar Cells with Enhanced Open-Circuit-Voltage and Suppressed Charge Recombination. *Nano Energy* **2018**, *44*, 155−163.
(68) Bao, X.; Zhang, Y.; Wang, J.; Zhu, D.; Yang, C.; Li, Y.; Yang, C.; Xu, J.; Yang, R. High Extinction Coefficient Thieno[3,4-b]Thiophene-Based Copolymer for Efficient Fullerene-Free Solar Cells with Large Current Density. *Chem. Mater.* **2017**, *29*, 6766−6771.
(69) Xue, X.; Weng, K.; Qi, F.; Zhang, Y.; Wang, Z.; Ali, J.; Wei, D.; Sun, Y.; Liu, F.; Wan, M.; Liu, J.; Huo, L. Steric Engineering of Alkylthiolation Side Chains to Finely Tune Miscibility in Nonfullerene Polymer Solar Cells. *Adv. Energy Mater.* **2018**, 1802686.
(70) Liu, Z.; Gao, Y.; Dong, J.; Yang, M.; Liu, M.; Zhang, Y.; Wen, J.; Ma, H.; Gao, X.; Chen, W.; Shao, M. Chlorinated Wide-Bandgap Donor Polymer Enabling Annealing Free Nonfullerene Solar Cells with the Efficiency of 11.5%. *J. Phys. Chem. Lett.* **2018**, *9*, 6955−6962.
(71) Li, W.; Ye, L.; Li, S.; Yao, H.; Ade, H.; Hou, J. A High-Efficiency Organic Solar Cell Enabled by the Strong Intramolecular Electron Push-Pull Effect of the Nonfullerene Acceptor. *Adv. Mater.* **2018**, *30*, 1707170.
(72) Chen, S.; Lee, S. M.; Xu, J.; Lee, J.; Lee, K. C.; Hou, T.; Yang, Y.; Jeon, M.; Lee, B.; Cho, Y.; Jung, S.; Oh, J.; Zhang, Z.-G.; Zhang, C.; Xiao, M.; Li, Y.; Yang, C. Ultrafast Channel II Process Induced by a 3-D Texture with Enhanced Acceptor Order Ranges for High-Performance Non-Fullerene Polymer Solar Cells. *Energy Environ. Sci.* **2018**, *11*, 2569−2580.

DOI: 10.1021/acsami.8b19449
ACS Appl. Mater. Interfaces 2019, 11, 9239−9250